remote sensing

MDPI

Letter

Inter-Comparison of Normalized Difference Vegetation Index Measured from Different Footprint Sizes in Cropland

Jae-Hyun Ryu [1], Sang-Il Na [2] and Jaeil Cho [1,*]

[1] Department of Applied Plant Science, Chonnam National University, 77 Yongbong-ro, Gwangju 61186, Korea; 167334@jnu.ac.kr or ryu.jaehyun88@gmail.com

[2] National Institute of Agricultural Sciences, Rural Development Administration, Wanju 55365, Korea; sangil917@korea.kr

* Correspondence: chojaeil@jnu.ac.kr; Tel.: +82-62-530-2056; Fax: +82-62-530-2059

Received: 24 July 2020; Accepted: 11 September 2020; Published: 14 September 2020



Abstract: Remote sensing techniques using visible and near-infrared wavelengths are useful for monitoring terrestrial vegetation. The normalized difference vegetation index (NDVI) is a widely used proxy of vegetation conditions, and it has been measured at various footprint sizes using satellite, unmanned aerial vehicle (UAV), and ground-installed sensors. The goal of this study was to analyze the spatial characteristics of NDVI data by comparing the values obtained at different footprint sizes. In particular, the NDVI was evaluated in garlic and onion fields that featured ridges and furrows. The evaluation was performed using data from a leaf spectrometer, field spectrometers, ground-installed spectral reflectance sensors, a multispectral camera onboard a UAV, and Sentinel-2 satellites. The correlation coefficients between NDVIs evaluated from the various sensors (excluding the satellite-mounted sensors) ranged from 0.628 to 0.944. The UAV-based NDVI ($NDVI_{UAV}$) exhibited the lowest root mean square error (RMSE = 0.088) when compared with field spectrometer data. On the other hand, the satellite-based NDVI data ($NDVI_{Sentinel-2}$) were poorly correlated with those obtained from the other sensors as a result of the footprint mismatch. However, by upscaling the $NDVI_{UAV}$ data to the pixel size of Sentinel-2, the comparison was improved, and the following statistics were obtained: correlation coefficient: 0.504–0.785; absolute bias: 0.048–0.078; RMSE: 0.063–0.094. According to the aforementioned results, ground-based NDVI data can be used to validate $NDVI_{UAV}$ data without further processing and $NDVI_{UAV}$ data can be used to validate $NDVI_{Sentinel-2}$ data after upscaling to the Sentinel-2 pixel size. Overall, the results presented in this study may be helpful to understand and integrate NDVI data at different spatial scales.

Keywords: NDVI; spectrometer; unmanned aerial vehicle; satellite; footprint; spatial scale

1. Introduction

The reflection of visible and near-infrared (NIR) wavelengths, captured by means of remote sensing techniques, has been widely used to nondestructively monitor various characteristics and patterns of vegetation [1]. The spectral reflectance of blue and red wavelengths decreases, while that of the NIR wavelengths increases as the biomass of healthy vegetation increases [2]. The spectral reflectance has been used to calculate vegetation indices. Among them, the normalized difference vegetation index (NDVI) has been utilized to detect crop production [3], change in vegetation phenology due to climate change [4], effects of disasters such as forest fires [5], and agricultural drought [6].

In particular, the utilization of satellite data for precision agriculture increased after the launch of the Sentinel-2 satellites, which carries sensors for wavelengths that are useful for producing vegetation

indices [7]. Two satellites, Sentinel-2A and Sentinel-2B, were launched in June 2015 and March 2017, respectively. Their combined temporal resolution period was 5 days [8]. Nevertheless, surface information sometimes cannot be acquired because of interference by clouds, aerosols, moisture, or fog. Moreover, monitoring a crop in the booting stage is difficult, and so is identifying vegetation conditions under stress related to a disease or a heatwave [9,10]. Some studies argue that satellite data with higher spatial resolution are required for precision agriculture [9,11].

These limitations can be overcome using unmanned aerial vehicle (UAV)-based remote sensing techniques. Multispectral cameras on UAVs can capture data that are useful for evaluating vegetation conditions [12,13]. A UAV can cover comparatively small areas, but can provide data with a ground sample distance (GSD) of a few centimeters, thereby offering improved spatial resolution compared with that of satellites [14]. Moreover, UAVs offer flexible measurement schedules [11,15].

NDVI values measured from satellite and UAV data were compared to those obtained from ground-installed sensors and field spectrometers (or handheld spectrometers) [16,17]. Ground-based data are normally considered as "true reference sources" owing to the fact that the distance between the sensor and the measurement target is small. Ground-based remote sensing data show minimal atmospheric effects at altitudes lower than 10 m [18]. Given that scans of ground-installed optical devices are frequent [19], these devices can provide information on the crop condition continually. Meanwhile, spectral information obtained at different spatial scales can enable a comprehensive characterization of the vegetation in a target area. Ground-based vegetation data may reflect the spectral characteristics of a crop growing on homogeneous land. However, satellite-based data can provide information on heterogeneous land types. In particular, the presence of ridges and furrows can affect the comparison of data from different sources [15]. Therefore, the spatial characteristics of the data obtained from ground-based, airborne, and spaceborne sensors should be taken into account when making comparisons across data. In previous studies, the spatial characteristics of vegetation indices were only compared under specific spatial scales: comparisons between UAV and satellite data [15,20] or between ground-based data and satellite data [16] were carried out.

The purpose of this study is to compare NDVI values obtained at different spatial scales (from 5.5 mm to 10 m) in garlic and onion cropland to understand their spatial characteristics. The NDVI data used in this study were obtained from ground-based sensors (a leaf spectrometer, field spectrometers, and spectral reflectance sensors (SRSs)), a multispectral camera onboard a UAV, and a multispectral instrument mounted on a satellite. The NDVI values were compared using statistical metrics. Next, the UAV-based NDVI data were upscaled to the pixel size of the satellite-based NDVI data to evaluate how the results of the comparison changed.

2. Materials and Methods

2.1. Study Area and Crops

The study area (34.968°N, 126.4515°E) is a plot of land at the Bioenergy Crop Research Institute in Muan County, South Korea. Garlic and onion were being cultivated in this plot. They are considered representative vegetable crops in South Korea as they are the essential ingredients for almost every delicacy (including Kimchi, a typical Korean food) [21]. The crops were cultivated from October 2017 to June 2018. In particular, the garlic cultivars *Hongsan*, *Namdo*, and *Daeseo* and the onion cultivar *Sunpower* were used. The ridges and furrows were 1.2 m and 0.6 m long, on average. In the garlic field, the planting distance was 13 cm and nine plants were cultivated in each row. In the onion field, the planting distance was 15 cm and six plants were cultivated in each row. Garlic and onion begin to grow during autumn, then enter a dormant stage in winter in response to the low air temperature, and resume their growth in spring. In the study area, the mean (2001–2019) air temperature was 13.42 °C and the mean cumulative precipitation was 1282.5 mm/year according to data collected at Muan station, an automatic weather station of the Korea Meteorological Administration located approximately 2 km from the study area.

2.2. Ground-Based Remote Sensing Measurements

Ground-based remote sensing measurements were performed using a handheld leaf spectrometer, handheld field spectrometers, and ground-installed SRSs to obtain NDVI data. In particular, the leaf spectrometer (CID CI-710, Bio-Science, Camas, WA, USA) was used to obtain spectral reflectance information on garlic at a leaf spatial scale at three locations (G1, G2, and G3, see Figure 1a). This device can measure the spectral reflectance in the range of 400–950 nm with a sampling interval smaller than 0.215 nm. The diameter of the leaves on which the leaf spectrometer measurements were performed was 5.5 mm. The measurements were repeated three times on each leaf, and 10 leaves were measured at each site to obtain a representative measure of the crop condition.

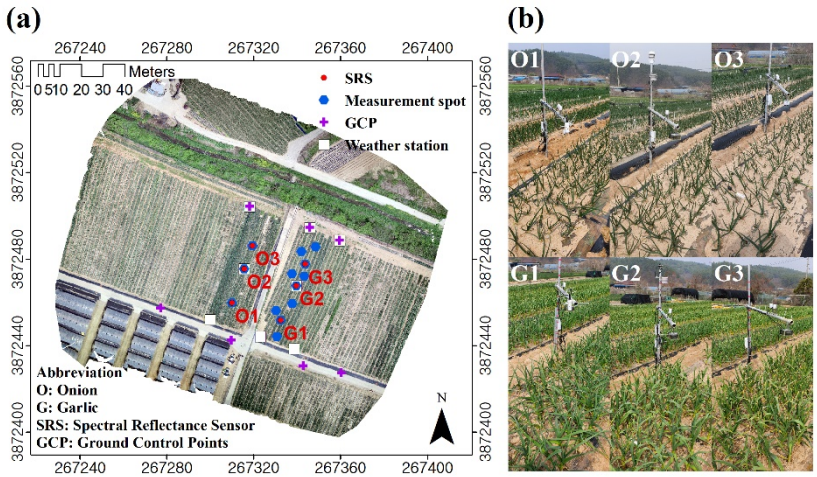


Figure 1. (**a**) Positions of the SRSs and optical measurement points; (**b**) photographs of SRSs at each position.

Two field spectrometers (AvaSpec-UL2048L, Avantes BV, Apeldoorn, The Netherlands) were used to monitor the crops at visible and NIR wavelengths (from 350 to 1050 nm). The sampling interval at 700 nm was 0.576 nm. The field of view (FOV) of the bare fiber-mounted field spectrometer was 23°. One field spectrometer was used to monitor the sunlight reflected by a white reference panel (RS50 White Reflectance Standard, StellarNet Inc., Tampa, FL, USA) that provided > 97% reflectivity of visible and NIR wavelengths. The other field spectrometer was used to monitor the light reflected from the crops at a height of 70 cm from the crop canopy. The measurements were averaged over 10 observations to minimize the observation error; three samples at each position were monitored to obtain representative results of the crop conditions. In particular, measurements were conducted at 13 locations during solar noon. The reflectance was calculated using irradiance and radiance data, which were recorded simultaneously. In addition, cross-calibration values were applied over the entire range of wavelengths monitored by the two spectrometers.

The leaf and field spectrometer measurements were conducted immediately after or before the UAV measurements to ensure correspondence across the data [19]. The NDVI values were calculated from the spectral reflectance converted to 1 nm intervals, as follows: $NDVI = (R_{840} - R_{665})/(R_{840} + R_{665})$, where R_{840} and R_{665} are the spectral reflectance values for 10 nm of bandwidth.

The SRSs (METER Group, Inc., Pullman, WA, USA) were installed near the ground surface to monitor the crop conditions at six locations continually (Figure 1b). The SRSs working at 650 nm and 810 nm (with 10 nm of bandwidth) are based on photodiode sensors and consist of upward- and downward-facing sensors with FOVs of 180° and 36°, respectively. The SRS data were stored in data loggers (EM50, METER Group, Inc., Pullman, USA) every 2 min. The distance between an SRS and the plant canopy was approximately 70 cm and the height of the downward-facing sensor was adjusted to maintain a constant distance by accounting for the plant height. The NDVI was calculated from

data measured from 11:00 to 14:00 local time in order to minimize the solar zenith angle for each day. The SRS-based daily mean NDVI (hereafter $NDVI_{SRS}$) was obtained after excluding the 15% largest and 15% smallest NDVI values.

2.3. UAV-Based Remote Sensing Measurements

The eight-propeller DJI S1000 UAV (SZ DJI Technology Co., Ltd., Sham Chun, Guangdong Province, China), equipped with a multispectral camera (RedEdge, Micasense, Inc., Seattle, WA, USA), was used in this study [22]. This multispectral camera has blue (center wavelength: 475 nm; bandwidth: 20 nm), green (560 nm; 20 nm), red (668 nm; 10 nm), red edge (717 nm; 10 nm), and NIR (840 nm; 40 nm) bands, which were used to evaluated the NDVI (hereafter UAV_{NDVI}). The FOV (imager resolution) of the multispectral camera was 47.2° (1280 × 960 pixels).

The UAV-based remote sensing measurements were conducted four times after the dormant stage of garlic and onion (Table 1). The flight altitude was set to 30 m with a mean GSD of approximately 2.18 cm (multispectral camera), with 80% forward and sideways overlap. The UAV-based raster data were obtained at solar noon. A calibrated reflectance panel (Micasense, Inc.) was utilized to obtain the reflectance data from the multispectral camera. The UAV-based imagery was processed using Pix4D software (version 4.3.31). Information on the seven ground control points (GCPs) was obtained using a GRX2 GNSS Receiver (SOKKIA Corporation, Olathe, KS, USA).

Table 1. Measurement information for ground-, unmanned aerial vehicle (UAV-), and satellite-based remote sensing techniques.

Number	Measurement Date	Ground	Airborne	Satellite	Time Difference [a]
		Leaf- and Field-Spectrometer	UAV	Sentinel-2	
1	28 Mar. 2019	O	O [b]	-	−1 day
	29 Mar. 2019	-	-	O	+1 day
2	16 Apr. 2019	O	O [c]	-	−2 days
	18 Apr. 2019	-	-	O	+2 days
3	3 May 2019	O	O [d]	O	0 day
4	13 May 2019	-	-	O	−4 days
	17 May 2019	O	O [e]	-	+4 days

[a] Time difference between satellite and ground/airborne measurements. Measurement time (hh:mm) of UAV: b, 12:41–12:50; c, 14:14–14:25; d, 11:52–12:00; e, 12:13–12:22.

2.4. Satellite-Based Remote Sensing Measurements

High-resolution satellite data are useful for the continuous monitoring of cropland at a regional scale. In this study, data from the multispectral instrument (MSI) onboard Sentinel-2 were compared with the ground- and UAV-based NDVI values obtained for the cropland in the study area.

Sentinel-2 data were downloaded from the Copernicus Hub of the European Space Agency (ESA) [23]. Level-2A data of Sentinel-2/MSI from March 2019 to May 2019 were obtained, on which geometric processing and atmospheric correction were performed. The data covered a target area that included the study area. NDVI values (hereafter $NDVI_{Sentinel\text{-}2}$) were calculated from the reflectance in band 4 (red; center wavelength: 665 nm; bandwidth: 30 nm) and band 8 (NIR; 842 nm; 115 nm) after excluding cloud pixels through a scene classification map. The spatial resolution of Sentinel-2/MSI is 10 m in the red and NIR bands. Four dates were selected to perform the comparison with the ground- and UAV-based data: 29 March 2019, 18 April 2019, 3 May 2019, and 13 May 2019 (Table 1). The time differences between the UAV and satellite measurements were 1, 2, 0, and 4 days, respectively. These differences were deemed acceptable, as the NDVI values of garlic and onion crops do not change significantly during a few days under non-stress conditions.

2.5. Methods Used to Compare the Values Measured at Different Spatial Scales

To allow for objective comparisons, a set of criteria was adopted. In particular, two approaches were followed. In the first approach, the NDVI values were calculated from the data obtained by the ground-based sensors without further processing. In contrast, the UAV-based remote sensing data were first averaged over the pixels belonging to a region of interest (ROI) using the geospatial data abstraction library. The ROI was set at each ground measurement spot as a diameter (area) of approximately 82.0 cm (0.528 m^2) considering the length of a ridge and the geolocation error of the $NDVI_{UAV}$ data. The Sentinel-2/MSI-based data were extracted using the nearest neighbor method for each spot. The correlation coefficient, absolute bias, and root mean square error (RMSE) were used to evaluate the relationships among the NDVI values measured at different spatial scales. A bias-corrected RMSE was also calculated.

The second approach entailed the upscaling of the UAV data to the scale of the Sentinel-2/MSI data. Figure 2 shows the NDVI map acquired using UAV and satellite data. The background of Figure 2 shows the $NDVI_{Sentinel-2}$ and $NDVI_{UAV}$ data overlapped over the $NDVI_{Sentinel-2}$ data. The grey lines indicate the boundaries of the pixels of the $NDVI_{Sentinel-2}$ data. The blue grids indicate the selected ROI based on the Sentinel-2 pixels, which represent the cropland. The $NDVI_{UAV}$ values were averaged over the Sentinel-2 pixels (each blue pixel). This calculation yielded "upscaled $NDVI_{UAV}$ values" [24]. The relationship between the upscaled $NDVI_{UAV}$ and the $NDVI_{Sentinel-2}$ values was evaluated (in terms of the homogeneity of one pixel) through a coefficient of variation (CV), which was calculated as the standard deviation divided by the mean value. Additionally, the normalized RMSE (NRMSE) was calculated as $RMSE/(Y_{max.} - Y_{min.}) \times 100$ to understand the relative difference of the errors in the four measurement dates. $Y_{max.}$ and $Y_{min.}$ are the maximum and minimum values, respectively, of the variable on the y-axis.

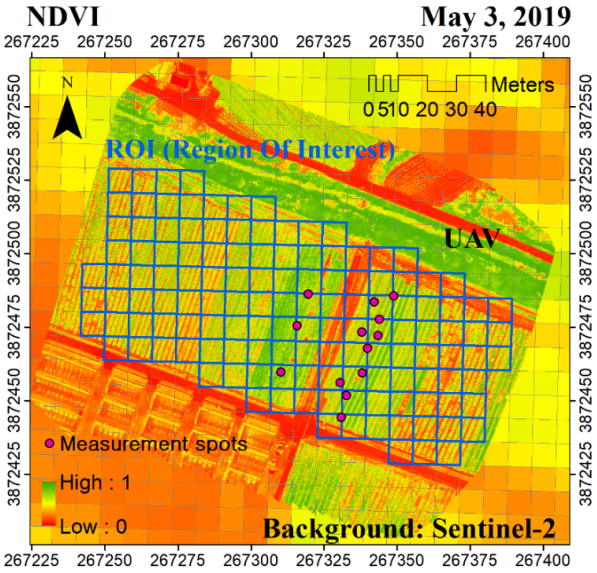


Figure 2. Sentinel-2 and UAV-based normalized difference vegetation index (NDVI) maps for 3 May 2019. The gray grid indicates the pixel boundaries of Sentinel-2 and the blue grid indicates the ROI used to compare the $NDVI_{UAV}$ and $NDVI_{Sentinel-2}$ data.

3. Results

3.1. Comparison of NDVI Data

The NDVI values obtained from the leaf spectrometer (hereafter $NDVI_{Leaf}$) ranged from 0.694 to 0.814 from March to May 2019. The field spectrometer-based NDVI (hereafter $NDVI_{Field}$) and $NDVI_{SRS}$ increased after the dormant stage (i.e., during winter) and decreased between mid-April and early May.

$NDVI_{Field}$ and $NDVI_{SRS}$ values decreased earlier in the garlic field than in the onion field. The growth and lodging of onion in the enlargement stage (i.e., during spring) increased the fraction of vegetation in the measurement area, maintaining a high NDVI value in the onion field. The $NDVI_{UAV}$ values clearly indicated vegetation and non-vegetation areas (Supplementary Materials Figure S1). The concrete roads and greenhouse areas exhibited low NDVI values (<0.1 and 0.4, respectively). In addition, throughout the measurement period, artificial structures yielded the same range of NDVI values.

The relationships among the NDVI values evaluated at different spatial scales are shown in Figure 3. $NDVI_{UAV}$ had correlation coefficients as high as 0.933 (p-value < 0.0001) and 0.944 (p-value < 0.0001) with $NDVI_{Field}$ and $NDVI_{SRS}$, respectively. In particular, the absolute bias between $NDVI_{UAV}$ and $NDVI_{Field}$ was just 0.069. In addition, the bias-corrected RMSEs of $NDVI_{UAV}$ were 0.046 and 0.051 with $NDVI_{Field}$ and $NDVI_{SRS}$, respectively. Although a bias existed between $NDVI_{Field}$ and $NDVI_{SRS}$, a high correlation coefficient was obtained (R = 0.901, p-value < 0.0001). After excluding the bias between $NDVI_{Field}$ and $NDVI_{SRS}$, a bias-corrected RMSE of 0.077 was obtained. $NDVI_{Leaf}$ had correlation coefficients of 0.628 (p-value < 0.0288), 0.724 (p-value < 0.0078), and 0.836 (p-value < 0.0007) with $NDVI_{UAV}$, $NDVI_{Field}$, and $NDVI_{SRS}$, respectively.

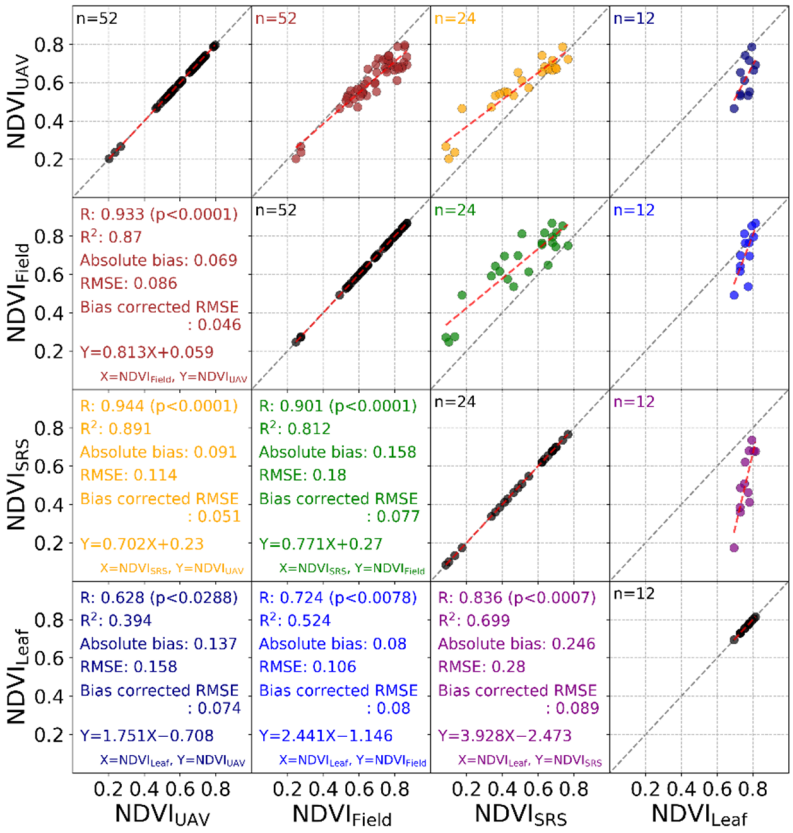


Figure 3. Pair plots for $NDVI_{UAV}$, $NDVI_{Field}$, $NDVI_{SRS}$, and $NDVI_{Leaf}$. The p-value is <0.05 for each relationship. RMSE, root mean square error.

The ground- and UAV-based NDVI values were compared with the satellite-based NDVI values (Figure 4). $NDVI_{SRS}$ had a relatively high correlation coefficient (0.692, p-value < 0.0002) with $NDVI_{Sentinel\text{-}2}$. The reason for this was assumed to be that $NDVI_{SRS}$ was evaluated over a relatively homogeneous area because the SRS was installed in the middle of the cropland even though ridges and furrows were included (Figure 1). Meanwhile, the correlation coefficient between $NDVI_{Sentinel\text{-}2}$ and the other NDVI values at different spatial scales was low. In particular, there was no statistical significance with $NDVI_{Leaf}$ (p-value < 0.8414).

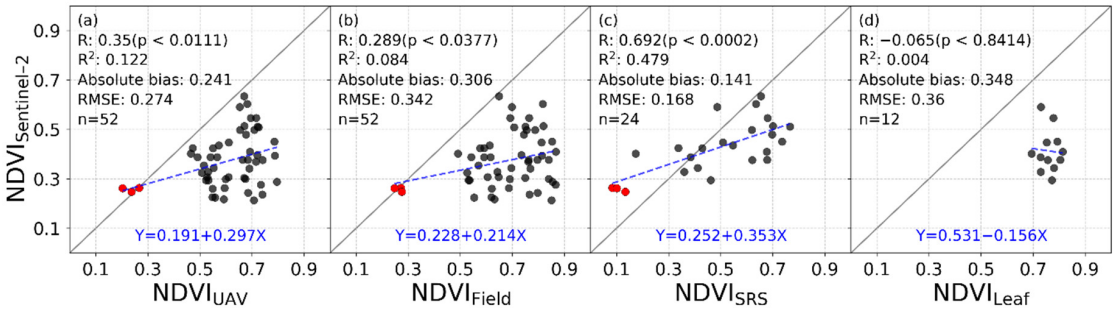


Figure 4. Relationship between $NDVI_{Sentinel-2}$ and (**a**) $NDVI_{UAV}$, (**b**) $NDVI_{Field}$, (**c**) $NDVI_{SRS}$, and (**d**) $NDVI_{Leaf}$ within the ROI. The blue dotted line refers to all data marked by circles. The red circles refer to the measurement data for the onion field on 28 March 2019.

The red circles in Figure 4 refer to onion field data from 28 March 2019. At that time, the vegetation fraction was low (Figure S3). If the red circles are excluded, the correlation coefficients of $NDVI_{UAV}$, $NDVI_{Field}$, and $NDVI_{SRS}$ with $NDVI_{Sentinel-2}$ decrease to 0.239 (p-value < 0.0983), 0.151 (p-value < 0.2992), and 0.467 (p-value < 0.0327), respectively. In particular, the statistical significances of $NDVI_{UAV}$ and $NDVI_{Field}$ with $NDVI_{Sentinel-2}$ were low except for the red circles on 28 March 2019.

3.2. Comparison of Upscaled $NDVI_{UAV}$ and $NDVI_{Sentinel-2}$ Data

$NDVI_{UAV}$ data were upscaled to the Sentinel-2 pixel size to evaluate possible improvements in the correlation with $NDVI_{Sentinel-2}$. A sample (135 pixels) in the ROI that represented cropland was selected (Figure S2). The correlation coefficients between upscaled $NDVI_{UAV}$ and $NDVI_{Sentinel-2}$ on 28 March, 16 April, 3 May, and 13 May of 2019 were 0.596 (p-value < 0.0001), 0.504 (p-value < 0.0001), 0.785 (p-value < 0.0001), and 0.776 (p-value < 0.0001), respectively (Figure 5). The correlation coefficients increased in the later stage of crop growth. The correlation between these two NDVI data series was relatively low in March and April (Figure 5a,b). However, some pixels exhibited high CV values on 28 March 2019 (Figure 5a), implying that each pixel could contain heterogeneous land types (e.g., cropland and bare soil). The NRMSE and the bias-corrected NRMSE were 22.4%. The correlation coefficient between the two NDVI data series was the lowest on 16 April 2019 (Figure 5b). The NRMSE and the bias-corrected NRMSE were 21.8% and 19.8%, respectively, and these results were similar to the values obtained in March. The best results were obtained on 3 May 2019, when the NRMSE and bias-corrected NRMSE were 16.7% and 13.4%, respectively (Figure 5c).

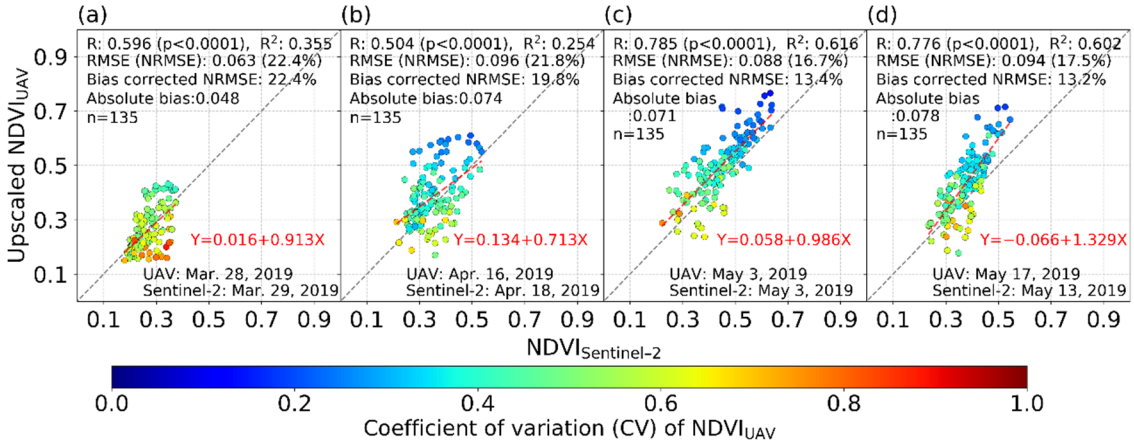


Figure 5. Relationship between upscaled $NDVI_{UAV}$ and $NDVI_{Sentinel-2}$ on (**a**) 28 March 2019, (**b**) 16 April 2019, (**c**) 3 May 2019, and (**d**) 13 May 2019. NRMSE, normalized RMSE.

The NDVI values obtained from UAV and satellite data on 3 May 2019 were the highest during the growth period, implying that the vegetation-covered area was the largest in this period (Figures S3 and S4). The UAV and satellite measurements in this period were recorded on the same day. The correlation coefficient for the last measurement (13 May 2019) was similar to that evaluated on 3 May 2019. The NRMSE and bias-corrected NRMSE were 17.5% and 13.2%, respectively. This implies that, by accounting for the bias between $NDVI_{UAV}$ and $NDVI_{Sentinel\text{-}2}$, a reasonably strong correlation between the upscaled $NDVI_{UAV}$ and $NDVI_{Sentinel\text{-}2}$ could be obtained when the vegetation-covered area was high. The correlation coefficient, RMSE, and absolute bias on the total measurement were 0.817, 0.086, and 0.068, respectively. Upscaled $NDVI_{UAV}$ values were generally higher compared with the $NDVI_{Sentinel\text{-}2}$ values in the cropland that included ridges and furrows.

4. Discussion

The different footprint sizes of the sensors can be deemed attributable for the differences in NDVI values and ranges. The NDVI is a proxy for the structural condition of vegetation. In particular, $NDVI_{Leaf}$ values refer to areas fully covered by vegetation (i.e., to individual leaves), even though the NDVI includes chlorophyll information from the red band data [25]. Therefore, the range of variation of the $NDVI_{Leaf}$ values is smaller compared with that of the NDVI values obtained from the other sensors.

All comparisons between couples of NDVI data series from different sensors are statistically significant, with the exception of those involving $NDVI_{Sentinel\text{-}2}$ data (Figure 3). In particular, $NDVI_{UAV}$ had a correlation coefficient higher than 0.933 (p-value <0.0001) with $NDVI_{Field}$ and $NDVI_{SRS}$. This implies that the $NDVI_{UAV}$ values are reliable in clear sky conditions. On the contrary, $NDVI_{Leaf}$, $NDVI_{Field}$, and $NDVI_{UAV}$ are not significantly correlated with $NDVI_{Sentinel\text{-}2}$. It should be noted that the spatial resolution of Sentinel-2 is approximately 10 m, implying that each pixel of a Sentinel-2 image comprises both crop and bare soil areas owing to the presence of ridges and furrows. However, by upscaling the $NDVI_{UAV}$ data to the pixel size of Sentinel-2, the correlation coefficient with $NDVI_{Sentinel\text{-}2}$ increased to 0.504–0.785.

In previous studies, $NDVI_{UAV}$ and $NDVI_{Sentinel\text{-}2}$ were reported to exhibit correlation coefficients of 0.55–0.72 in a vineyard [15]. Di Gennaro et al. [20] also reported R-square values of 0.57–0.80 between NDVIs evaluated from a UAV-mounted sensor and from Sentinel-2 in a vineyard. In another study, not only Sentinel-2 data, but Landsat-8 data as well were compared with ground and UAV data. $NDVI_{UAV}$ had an R-square value of 0.93 and 0.86 with NDVIs evaluated from ground and Landsat-8 data (hereafter $NDVI_{Landsat\text{-}8}$), respectively, in mixed deciduous and coniferous woodland [26]. In particular, the relationship between $NDVI_{UAV}$ and $NDVI_{Landsat\text{-}8}$ at the beginning of spring was relatively weak (R-square < 0.5), and the authors noted that this was due to a temporal gap between the Landsat and UAV data [27]. In fact, according to Battude et al. [28], high correlation coefficients between NDVIs using different satellites were evaluated if there was no temporal gap between the measurements. Indeed, in the present study, the bias-corrected NRMSE values were the lowest when data acquired on the same day by different sensors were compared (Figure 5).

Furthermore, NDVI values obtained from MODIS sensor data recorded by the Terra satellite, which has a relatively lower spatial resolution compared with Sentinel-2 and Landsat-8, showed different relationships depending on the land type [29]. In cropland, the R-square between NDVIs evaluated from ground sensor data and MODIS data was 0.55–0.56.

Each relationship between NDVI data series carried a distinct bias due to different measurement intervals, meteorological conditions, and different sensor specifications (FOV, sensor calibration, distance between the target and the sensor) [30,31]. In addition, the wavelength ranges used for calculating the NDVI were different depending on the optical instruments. For the red band, the central wavelength was 650 nm (bandwidth: 10 nm) for the SRS, while it was 665 nm or 668 nm (bandwidth: 10 nm or 30 nm) for the other instruments. It was calculated that this produced an absolute bias in the comparison between $NDVI_{SRS}$ and $NDVI_{Field}$ values of as high as 10% (result not shown). It also implies that the influence of other specifications is larger than that of the wavelength range. The FOV

of the field spectrometer is narrower than that of the SRS, implying that the field spectrometer data are more focused on the center of the crop. To reduce the bias, a bias correction method should be implemented, corresponding to the reference study. As for the relationship between $NDVI_{Sentinel-2}$ and upscaled $NDVI_{UAV}$, the error may originate from different georeferencing of the satellite and UAV data. Inherently, mosaicking and georeferencing UAV data in cropland and forests are relatively difficult tasks [19,32]. To alleviate this issue, multiple and accurate GCP target points must be installed.

5. Conclusions

NDVI values obtained at different spatial scales were compared in this work. The statistical analysis of the NDVI values obtained from the multispectral camera, field spectrometers, SRSs, and leaf spectrometer demonstrated that measurements with similar footprint areas are comparable. Moreover, the different footprint areas caused the $NDVI_{Sentinel-2}$ values to differ significantly from those evaluated from airborne and ground-based sensors ($NDVI_{UAV}$, $NDVI_{Field}$, $NDVI_{SRS}$, and $NDVI_{Leaf}$). Given that the correlation coefficient between $NDVI_{UAV}$ and $NDVI_{SRS}$ or $NDVI_{Field}$ data is higher than 0.933 (p-value < 0.0001), it was concluded that $NDVI_{SRS}$ and $NDVI_{Field}$ can be used as a true reference source for homogeneous crop-canopy areas. As for the relationship between $NDVI_{UAV}$ and $NDVI_{Sentinel-2}$, the upscaled $NDVI_{UAV}$ values (i.e., $NDVI_{UAV}$ values upscaled to the pixel size of Sentinel-2) exhibited a better correlation with the $NDVI_{Sentinel-2}$ values compared with the non-upscaled $NDVI_{UAV}$ values. This was attributed to the fact that the upscaled $NDVI_{UAV}$ had the same footprint area as $NDVI_{Sentinel-2}$, and suggested that the footprint mismatch is the most critical issue hindering proper data integration from different sensors and across spatial scales. For practical applications in agriculture, resampling the UAV-based data is thus recommended rather than for the ground-based data to obtain comparable NDVI results. However, note that precise crop conditions with low soil contamination errors are better captured by ground-based sensors.

The results presented in this study may help to correctly interpret and compare NDVI maps obtained at different spatial scales. Further, this study also demonstrated that the presence of ridges and furrows must be taken into account when validating the measurement data. In the future, data at various spatial scales will be continually acquired to allow further comparisons of multiple remote-sensing-derived parameters for a variety of crops.

Supplementary Materials: The following are available online at http://www.mdpi.com/2072-4292/12/18/2980/s1, Figure S1: Maps of $NDVI_{UAV}$: The black grid indicates the ROI to compare the $NDVI_{UAV}$ and $NDVI_{Sentinel-2}$ on (a) 28 March 2019, 12:41; (b) 16 April 2019, 14:14; (c) 3 May 2019, 11:52; and (d) 17 May 2019, 12:13. Figure S2: Maps of $NDVI_{Sentinel-2}$ on (a) 29 March 2019, (b) 18 April 2019, (c) 3 May 2019, and (d) 13 May 2019. Figure S3: Pictures of onions at three SRS stations on 28 March, 16 April, 3 May, and 17 May of 2019. Figure S4: Pictures of garlic at three SRS stations on 28 March, 16 April, 3 May, and 17 May of 2019.

Author Contributions: All authors contributed this paper. J.-H.R., the main author, designed the research, measured and analyzed the remote sensing data, and wrote the manuscript; S.-I.N., the co-author, reviewed the paper and contributed to the discussion; J.C., the corresponding author, designed the research and wrote the manuscript. All authors have read and agreed to the published version of the manuscript.

Funding: This research was funded by the Rural Development Administration, grant number PJ013821032020.

Acknowledgments: The authors would like to thank the editors and the anonymous reviewers for their helpful comments.

Conflicts of Interest: The authors declare no conflict of interest.

References

1. Ali, M.M.; Al-Ani, A.; Eamus, D.; Tan, D.K.Y. Leaf nitrogen determination using non-destructive techniques—A review. *J. Plant Nutr.* **2016**, *40*, 928–953. [CrossRef]
2. Serrano, L.; Filella, I.; Peñuelas, J. Remote sensing of biomass and yield of winter wheat under different nitrogen supplies. *Crop Sci.* **2000**, *40*, 723–731. [CrossRef]
3. Ko, J.; Jeong, S.; Yeom, J.; Kim, H.; Ban, J.-O.; Kim, H.-Y. Simulation and mapping of rice growth and yield based on remote sensing. *J. Appl. Remote Sens.* **2015**, *9*, 096067. [CrossRef]

4. Buitenwerf, R.; Rose, L.; Higgins, S.I. Three decades of multi-dimensional change in global leaf phenology. *Nat. Clim. Chang.* **2015**, *5*, 364–368. [CrossRef]
5. Ryu, J.-H.; Han, K.-S.; Hong, S.; Park, N.-W.; Lee, Y.-W.; Cho, J. Satellite-based evaluation of the post-fire recovery process from the worst forest fire case in South Korea. *Remote Sens.* **2018**, *10*, 918. [CrossRef]
6. Kogan, F.N. Operational space technology for global vegetation assessment. *Bull. Am. Meteorol. Soc.* **2001**, *82*, 1949–1964. [CrossRef]
7. Clevers, J.; Kooistra, L.; van den Brande, M. Using sentinel-2 data for retrieving Lai and leaf and canopy chlorophyll content of a potato crop. *Remote Sens.* **2017**, *9*, 405. [CrossRef]
8. Navarro, G.; Caballero, I.; Silva, G.; Parra, P.-C.; Vázquez, Á.; Caldeira, R. Evaluation of forest fire on madeira island using sentinel-2A MSI imagery. *Int. J. Appl. Earth Obs. Geoinf.* **2017**, *58*, 97–106. [CrossRef]
9. Mulla, D.J. Twenty five years of remote sensing in precision agriculture: Key advances and remaining knowledge gaps. *Biosyst. Eng.* **2013**, *114*, 358–371. [CrossRef]
10. Moran, M.S.; Inoue, Y.; Barnes, E.M. Opportunities and limitations for image-based remote sensing in precision crop management. *Remote Sens. Environ.* **1997**, *61*, 319–346. [CrossRef]
11. Adão, T.; Hruška, J.; Pádua, L.; Bessa, J.; Peres, E.; Morais, R.; Sousa, J. Hyperspectral imaging: A review on UAV-based sensors, data processing and applications for agriculture and forestry. *Remote Sens.* **2017**, *9*, 1110. [CrossRef]
12. Barbedo, J.G.A. A review on the use of unmanned aerial vehicles and imaging sensors for monitoring and assessing plant stresses. *Drones* **2019**, *3*, 40. [CrossRef]
13. Li, J.; Zhang, F.; Qian, X.; Zhu, Y.; Shen, G. Quantification of rice canopy nitrogen balance index with digital imagery from unmanned aerial vehicle. *Remote Sens. Lett.* **2015**, *6*, 183–189. [CrossRef]
14. Jay, S.; Baret, F.; Dutartre, D.; Malatesta, G.; Héno, S.; Comar, A.; Weiss, M.; Maupas, F. Exploiting the centimeter resolution of UAV multispectral imagery to improve remote-sensing estimates of canopy structure and biochemistry in sugar beet crops. *Remote Sens. Environ.* **2019**, *231*, 110898. [CrossRef]
15. Khaliq, A.; Comba, L.; Biglia, A.; Ricauda Aimonino, D.; Chiaberge, M.; Gay, P. Comparison of satellite and UAV-based multispectral imagery for vineyard variability assessment. *Remote Sens.* **2019**, *11*, 436. [CrossRef]
16. Kim, J.; Ryu, Y.; Jiang, C.; Hwang, Y. Continuous observation of vegetation canopy dynamics using an integrated low-cost, near-surface remote sensing system. *Agric. For. Meteorol.* **2019**, *264*, 164–177. [CrossRef]
17. Ryu, J.H.; Oh, D.; Jang, S.W.; Jeong, H.; Moon, K.H.; Cho, J. Assessment of photochemical reflectance index measured at different spatial scales utilizing leaf reflectometer, field hyper-spectrometer, and multi-spectral camera with UAV. *Korean J. Remote Sens.* **2018**, *34*, 1055–1066.
18. Yu, X.; Liu, Q.; Liu, X.; Liu, X.; Wang, Y. A physical-based atmospheric correction algorithm of unmanned aerial vehicles images and its utility analysis. *Int. J. Remote Sens.* **2016**, *38*, 3101–3112. [CrossRef]
19. Padró, J.-C.; Muñoz, F.-J.; Ávila, L.; Pesquer, L.; Pons, X. Radiometric correction of landsat-8 and sentinel-2A scenes using drone imagery in synergy with field spectroradiometry. *Remote Sens.* **2018**, *101*, 1687. [CrossRef]
20. Di Gennaro, S.F.; Dainelli, R.; Palliotti, A.; Toscano, P.; Matese, A. Sentinel-2 validation for spatial variability assessment in overhead trellis system viticulture versus UAV and agronomic data. *Remote Sens.* **2019**, *11*, 2573. [CrossRef]
21. Oh, J.Y.; Kim, K.D. Control strategies for fungal pathogens on stored onion (*Allium cepa*) and garlic (*Allium sativum*): A review. *Life Sci. Nat. Resour. Res.* **2016**, *24*, 31–40.
22. Micasense Instruments Home Page. Available online: https://www.micasense.com (accessed on 7 April 2020).
23. Sentinel-Hub Home Page. Available online: https://apps.sentinel-hub.com/eo-browser (accessed on 31 December 2019).
24. Fisher, J.I.; Mustard, J.F. Cross-scalar satellite phenology from ground, Landsat, and MODIS data. *Remote Sens. Environ.* **2007**, *109*, 261–273. [CrossRef]
25. Sims, D.A.; Gamon, J.A. Relationships between leaf pigment content and spectral reflectance across a wide range of species, leaf structures and developmental stages. *Remote Sens. Environ.* **2002**, *81*, 337–354. [CrossRef]
26. Berra, E.F.; Gaulton, R.; Barr, S. Commercial off-the-shelf digital cameras on unmanned aerial vehicles for multitemporal monitoring of vegetation reflectance and NDVI. *IEEE Trans. Geosci. Remote Sens.* **2017**, *55*, 4878–4886. [CrossRef]

27. Berra, E.F.; Gaulton, R.; Barr, S. Assessing spring phenology of a temperate woodland: A multiscale comparison of ground, unmanned aerial vehicle and Landsat satellite observations. *Remote Sens. Environ.* **2019**, *223*, 229–242. [CrossRef]
28. Battude, M.; Al Bitar, A.; Morin, D.; Cros, J.; Huc, M.; Marais Sicre, C.; Le Dantec, V.; Demarez, V. Estimating maize biomass and yield over large areas using high spatial and temporal resolution Sentinel-2 like remote sensing data. *Remote Sens. Environ.* **2016**, *184*, 668–681. [CrossRef]
29. Hmimina, G.; Dufrêne, E.; Pontailler, J.-Y.; Delpierre, N.; Aubinet, M.; Caquet, B.; de Grandcourt, A.; Burban, B.; Flechard, C.; Granier, A.; et al. Evaluation of the potential of MODIS satellite data to predict vegetation phenology in different biomes: An investigation using ground-based NDVI measurements. *Remote Sens. Environ.* **2013**, *132*, 145–158. [CrossRef]
30. Lange, M.; Dechant, B.; Rebmann, C.; Vohland, M.; Cuntz, M.; Doktor, D. Validating MODIS and sentinel-2 NDVI products at a temperate deciduous forest site using two independent ground-based sensors. *Sensors* **2017**, *17*, 1855. [CrossRef]
31. Zhao, F.; Li, Y.; Dai, X.; Verhoef, W.; Guo, Y.; Shang, H.; Gu, X.; Huang, Y.; Huang, J. Simulated impact of sensor field of view and distance on field measurements of bidirectional reflectance factors for row crops. *Remote Sens. Environ.* **2015**, *156*, 129–142. [CrossRef]
32. Xiang, H.; Tian, L. Method for automatic georeferencing aerial remote sensing (RS) images from an unmanned aerial vehicle (UAV) platform. *Biosyst. Eng.* **2011**, *108*, 104–113. [CrossRef]



© 2020 by the authors. Licensee MDPI, Basel, Switzerland. This article is an open access article distributed under the terms and conditions of the Creative Commons Attribution (CC BY) license (http://creativecommons.org/licenses/by/4.0/).